A Time-Domain Approach to Band Formation in Periodic Media

Nishant Kashyap, Amit Tanwar, and Pragati Ashdhir*

Department of Physics, Hindu College,

University of Delhi, Delhi-110007, India

Vivek T. Ramamoorthy

School of Physics, Engineering, and Computer Science,

University of Hertfordshire, Hatfield AL10 9AB, United Kingdom

Abstract

Band formation in periodic media is a central topic in solid-state physics and is typically introduced using Bloch's theorem as an eigenvalue problem for infinite periodic systems. Although elegant, this approach assumes an idealized infinite lattice, shifts attention away from real-space wave dynamics, and presents band structures as static outcomes rather than emergent features of wave propagation. As a result, students often do not connect band gaps with familiar phenomena such as reflection, transmission, and interference, creating a disconnect between formal band theory and observable wave behavior. We address this problem by discussing how band gaps occur from wave propagation in finite periodic systems. A broadband wavepacket is launched into a layered medium using a staggered-grid finite-difference space-time algorithm, and the transmission spectra are used to identify band gaps. The Bloch dispersion relation and the exponential decay of the wave field within band gap regions are extracted, thus establishing a connection between real-space wave propagation and the Bloch description of periodic media.

I. INTRODUCTION

Wave propagation in periodic media exhibits strong frequency selectivity, leading to transmission bands separated by band gaps. This behavior is commonly introduced through Bloch's theorem and the Kronig–Penney model.[1,2] Although analytically appealing, these approaches emphasize the spectral properties of infinite systems and can make it difficult for students to connect the abstract band structure with familiar real-space wave dynamics.

In contrast, we show that band gaps emerge directly from real-space wave propagation as a consequence of phase-coherent multiple scattering. From this perspective, band structure is not introduced as an eigenvalue problem, but is discussed from time-domain measurements in finite systems, providing a physically transparent route to understanding.

To demonstrate this approach, we consider wave propagation in a finite periodic layered medium. A broadband wavepacket is launched into the structure, and its transmission is analyzed to reveal how frequency-dependent attenuation arises from multiple scattering and interference. The periodic lattice strongly attenuates waves in specific frequency ranges,

* pragatiashdhir@hinducollege.ac.in

known as stop bands.* This suppression becomes more pronounced as the number of layers in the lattice increases.

We use a finite-difference time-domain[3] formulation to simulate longitudinal elastic waves in one-dimensional composite structures,† whose material properties vary only along the direction of propagation. These structures have periodic variations in density or elastic stiffness, which lead to acoustic band gaps, which are closely analogous to electronic band structures in solids. The time-domain response enables direct extraction of transmission spectra, spatial decay within stop bands, and the Bloch dispersion relation.

Our approach provides a physically transparent connection between finite-system wave propagation and the band structure of periodic media, making the emergence of band gaps accessible in terms of interference and phase coherence. The accompanying Python implementations in the Supplemental Material are designed to support reproducibility and to facilitate integration into advanced undergraduate instruction.

II. TIME-DOMAIN MODEL FOR WAVE PROPAGATION

To examine how band formation emerges from wave propagation, we simulate the time evolution of longitudinal elastic waves in a one-dimensional periodic medium. In this medium, the density $\rho(x)$ and elastic modulus $E(x)$ vary piecewise along x, the direction of wave propagation.

The dynamics of this inhomogeneous system are described by the first-order velocity–stress equations[4,5]

$$\frac{\partial v}{\partial t} = \frac{1}{\rho(x)}\frac{\partial \sigma}{\partial x}, \tag{1}$$

$$\frac{\partial \sigma}{\partial t} = E(x)\frac{\partial v}{\partial x}, \tag{2}$$

where $v = \partial u/\partial t$ is the particle velocity, defined as the time derivative of the displacement field $u(x,t)$, and σ is the stress. The stress is related to the strain $\varepsilon = \partial u/\partial x$ by Hooke's law,

$$\sigma = E(x)\frac{\partial u}{\partial x}. \tag{3}$$

* In this work, the terms *band gap* and *stop band* are used interchangeably. More precisely, a band gap refers to the absence of propagating modes in an infinite periodic medium, while a stop band refers to the corresponding suppression of wave transmission in a finite periodic structure.

† Periodic composite materials that are designed to control, manipulate, and attenuate elastic waves are known as phononic crystals.

Equations (1) and (2) follow from basic principles of continuum mechanics. The time derivative of Eq. (3) gives Eq. (2).

To obtain Eq. (1), consider a small segment of the medium of length dx and cross-sectional area A. If the stresses acting on the two faces of the segment differ, the resulting imbalance produces a net force given by

$$F = A\left[\sigma(x+dx) - \sigma(x)\right] \approx A\,\frac{\partial \sigma}{\partial x}\,dx. \tag{4}$$

If we apply Newton's second law to this segment, the net force equals ma or mass times acceleration. The mass of the segment is $\rho(x)A\,dx$, and its acceleration is $\partial v/\partial t$, giving $ma = \rho(x)A\,dx\,\partial v/\partial t$. We equate ma to the force in Eq. (4) and obtain

$$\rho(x)\frac{\partial v}{\partial t} = \frac{\partial \sigma}{\partial x}, \tag{5}$$

which corresponds to Eq. (1). From Eqs. (1) and (2), wave propagation can be understood as a coupled exchange between particle motion and the internal forces acting between neighboring regions in the medium. A spatial variation of stress produces a net force that accelerates the material locally, as described by Eq. (1). Conversely, spatial variations in velocity correspond to deformation of the material (i.e., relative displacement between neighboring regions), which generates stress through the elastic response of the medium, as captured by Eq. (2). This mutual coupling between velocity and stress enables disturbances to propagate through the medium as elastic waves.

We solve Eqs. (1) and (2) using a staggered-grid finite-difference method based on the Yee algorithm.[6] In this formulation, different physical variables are stored at interleaved spatial locations to accurately represent wave propagation across material interfaces. The particle velocity v_i, associated with the motion of material elements, is defined at the nodal grid points i, whereas the stress $\sigma_{i+1/2}$, representing the force transmitted across adjacent cells, is defined at the interfacial positions $i+\frac{1}{2}$. This spatial staggering naturally aligns the discrete variables, v_i and $\sigma_{i+1/2}$, with their physical interpretation, improves the treatment of material discontinuities, and enhances the numerical accuracy and stability of wave propagation simulations in heterogeneous media.

The velocity v is defined at integer grid points and time steps (i, n),

$$v_i^n \approx v(i\Delta x, n\Delta t), \tag{6}$$

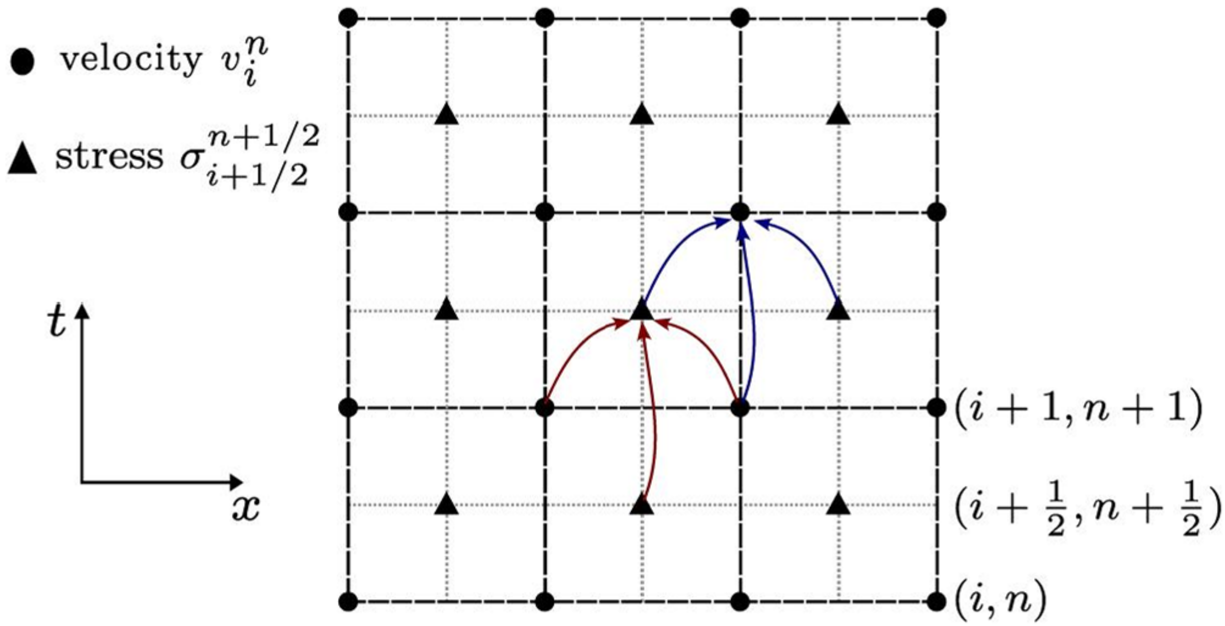

FIG. 1: Schematic of the staggered-grid arrangement. The velocity is defined at integer nodes, while the stress is defined at half-integer locations. The arrows indicate the alternating (leapfrog) update of the two fields.

and the stress σ is defined at half-integer grid points and time steps $(i+\frac{1}{2}, n+\frac{1}{2})$,

$$\sigma_{i+1/2}^{n+1/2} \approx \sigma\big((i+\tfrac{1}{2})\Delta x, (n+\tfrac{1}{2})\Delta t\big)\,. \tag{7}$$

Here, Δx and Δt are the spatial and temporal step sizes. This staggered arrangement is illustrated in Fig. 1.

The two fields are updated in an alternating (leapfrog) manner.[3] The time derivatives are approximated as

$$\left.\frac{\partial v}{\partial t}\right|_i^{n+1/2} \approx \frac{v_i^{n+1} - v_i^n}{\Delta t}, \tag{8}$$

and

$$\left.\frac{\partial \sigma}{\partial t}\right|_{i+1/2}^{n} \approx \frac{\sigma_{i+1/2}^{n+1/2} - \sigma_{i+1/2}^{n-1/2}}{\Delta t}. \tag{9}$$

The spatial derivatives are approximated by

$$\left.\frac{\partial v}{\partial x}\right|_{i+1/2}^{n} \approx \frac{v_{i+1}^{n} - v_i^n}{\Delta x}, \tag{10}$$

and

$$\left.\frac{\partial \sigma}{\partial x}\right|_i^{n+1/2} \approx \frac{\sigma_{i+1/2}^{n+1/2} - \sigma_{i-1/2}^{n+1/2}}{\Delta x}. \tag{11}$$

We substitute these derivatives into Eqs. (1) and (2); the stress is first updated using velocity values at time step n,

$$\sigma_{i+1/2}^{n+1/2} = \sigma_{i+1/2}^{n-1/2} + \left(\frac{E_{i+1/2}\Delta t}{\Delta x}\right)\left(v_{i+1}^{n} - v_i^{n}\right), \tag{12}$$

followed by the velocity update using the new stress values,

$$v_i^{n+1} = v_i^{n} + \left(\frac{\Delta t}{\rho_i \Delta x}\right)\left(\sigma_{i+1/2}^{n+1/2} - \sigma_{i-1/2}^{n+1/2}\right). \tag{13}$$

$E_{i+1/2}$ represents the elastic modulus at the interface between nodes i and $i+1$. It is evaluated using the harmonic mean of the adjacent nodal values. Physically, the adjacent grid cells act like two elastic springs connected in series. Because the stress must be continuous across the material boundary, their effective combined stiffness is correctly given by the harmonic mean. Using the harmonic mean in the evaluation of $E_{i+1/2}$ ensures an accurate representation of the interfacial stiffness, particularly when the elastic properties of neighboring materials differ significantly. The density ρ_i is defined at the velocity nodes.

Equations (12) and (13) form the discrete staggered-grid representation of Eqs. (1) and (2) and constitute the core of the numerical solver.

For numerical stability, the time step Δt must be chosen such that information carried by the fastest wave in the composite structure does not travel farther than one spatial grid interval Δx within a single time step. This requirement is expressed through the Courant–Friedrichs–Lewy (CFL) number α as

$$\Delta t = \alpha \frac{\Delta x}{c_{\max}}, \quad \text{with } \alpha < 1, \tag{14}$$

where $c_{\max}$ is the maximum wave speed in the medium. This condition ensures that the numerical update at any grid point depends only on neighboring points, consistent with the finite propagation speed of the wave. In this work, we take $\alpha = 0.98$ for all simulations, and the total number of time steps is fixed at 2^{18}.

Additionally, the spatial grid must be sufficiently fine to resolve the wave field correctly. This requirement is expressed by the number of grid points per wavelength N_{ppw}:

$$\Delta x = \frac{\lambda_{\min}}{N_{\text{ppw}}} \quad \text{with } \lambda_{\min} = \frac{c_{\min}}{f_{\max}}, \tag{15}$$

where $c_{\min}$ is the minimum wave speed in the medium and $f_{\max}$ is the highest frequency present in the source, so that $\lambda_{\min}$ is the smallest wavelength that must be resolved. N_{ppw} is the number of grid points used to represent one wavelength. This condition ensures that spatial variations of the wave field are accurately captured. In this work, $N_{\mathrm{ppw}} = 30$ is used to resolve the smallest wavelength in all simulations.

We now apply this framework to study band formation in periodic structures by considering a periodic lattice embedded in a surrounding medium. The system is excited using a broadband source placed in the surrounding medium before the lattice. A Ricker wavelet is used as the time-dependent source, defined as

$$s(t) = \left(1 - 2\pi^2 f_c^2 (t - t_c)^2\right) \exp\left[-\pi^2 f_c^2 (t - t_c)^2\right], \tag{16}$$

where f_c is the central frequency of the wavelet, t denotes time, and t_c is a time shift that determines when the pulse reaches its maximum amplitude. Because the Ricker wavelet is band-limited and has zero mean, it is well suited for transient wave simulations. The parameter f_c is chosen such that $f_c \approx 0.3\, f_{\max}$, ensuring that the significant frequency content of the source remains well within the frequency range resolved by the chosen spatial and temporal discretization. Choosing the source center frequency f_c significantly below $f_{\max}$, the highest frequency component present in the source, reduces errors associated with insufficient resolution and maintains an accurate representation of the wave field. The generated wavelet propagates through the domain according to Eqs. (12) and (13).

We record the velocity field[‡] at a fixed point in the surrounding medium beyond the lattice over the entire simulation time. The Fourier transform of this recorded signal is denoted by $v_{\mathrm{lattice}}(\omega)$, where $\omega = 2\pi f$ is the angular frequency corresponding to frequency f. The quantity $v_{\mathrm{lattice}}(\omega)$ represents the frequency components of the wave after propagation through the lattice. To isolate the frequency filtering effect of the periodic lattice, the same procedure is repeated for a uniform surrounding medium without the lattice. The corresponding Fourier transform, denoted by $v_{\mathrm{uniform}}(\omega)$, represents the frequency content of the excitation in the absence of the lattice. The transmission spectrum is then defined as the ratio of the magnitudes of the Fourier-transformed signals,

$$T(\omega) = \frac{|v_{\mathrm{lattice}}(\omega)|}{|v_{\mathrm{uniform}}(\omega)|}, \tag{17}$$

[‡] The stress field may also be used, as it contains equivalent wave information. The velocity field is chosen because it is defined at integer time steps in the staggered-grid method and can be recorded directly without interpolation.

which removes the influence of the source spectrum and retains only the frequency-dependent effect of the lattice, thereby highlighting the frequency ranges that are transmitted through or suppressed by the periodic structure.

For the analysis used to obtain the transmission spectrum, the surrounding medium is assumed to be unbounded, so that the wave field is influenced only by scattering from the lattice and not by boundary reflections. In the numerical model, however, the computational domain is finite and introduces artificial reflections at its boundaries. To suppress these reflections and mimic an unbounded medium, absorbing boundary conditions are applied at both ends of the spatial grid, allowing outgoing waves to exit the computational domain with minimal reflection. In this work, Mur's first-order absorbing boundary condition is used (see Appendix A).

The overall simulation procedure is summarized in Fig. 2. The layered structure and frequency range determine the spatial and temporal discretization, governed by the minimum points-per-wavelength resolution requirement defined by Eq. (15) and the Courant–Friedrichs–Lewy condition given by Eq. (14). The fields are then advanced in time using the staggered-grid method: at each time step, the stress field is first updated using Eq. (12), followed by the velocity update using Eq. (13). The source and absorbing boundary conditions are applied, and the velocity at the observation point is recorded. This sequence is repeated for the entire simulation duration. The recorded signals for both the periodic lattice and the corresponding uniform medium are then Fourier transformed, and the normalized transmission spectrum is calculated using Eq. (17) as the ratio of the periodic lattice spectrum to the uniform medium spectrum.

III. BAND FORMATION IN A FINITE PERIODIC LATTICE

We examine how frequency-dependent transmission arises from repeated wave scattering in a finite periodic lattice. The structure consists of six unit cells of alternating aluminum (Al) and epoxy (Ep) layers embedded in water, as shown in Fig. 3. The external boundaries between water and the layered region are denoted by Γ_1 and Γ_2, and the internal interfaces are denoted sequentially by I_1, I_2, I_3, and so on.

The thickness of each layer is chosen using the quarter-wavelength condition at a selected

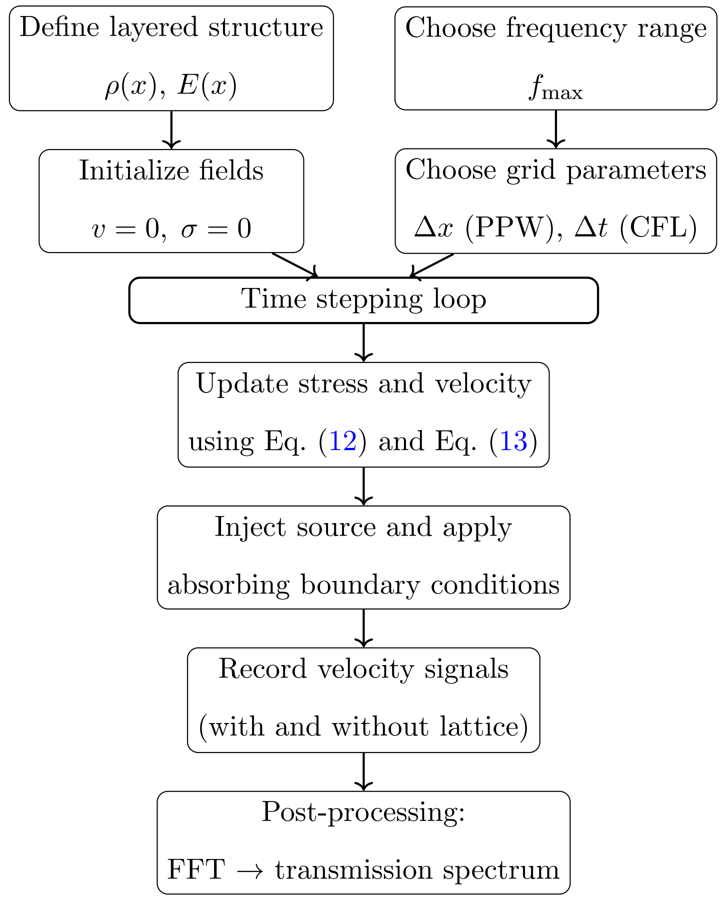

FIG. 2: Workflow of the time-domain simulation. The layered structure and chosen frequency range determine the spatial and temporal discretization as discussed in the text. The fields are advanced in time while injecting the source and applying absorbing boundary conditions. Velocity signals are recorded for both the periodic lattice and a uniform surrounding medium, and their Fast Fourier Transform is used to obtain the transmission spectrum by normalization.

reference frequency f_r. For each material i, the layer thickness d_i is defined as

$$d_i = \frac{\lambda_i}{4} = \frac{c_i}{4f_r}, \tag{18}$$

where $\lambda_i = c_i/f_r$ is the wavelength of a wave at frequency f_r in material i, and $c_i = \sqrt{E_i/\rho_i}$ is the longitudinal wave speed in that material. With this choice, a harmonic wave at frequency f_r accumulates a phase shift

$$k_i d_i = \frac{\pi}{2}, \tag{19}$$

while propagating across a single layer, where $k_i = 2\pi/\lambda_i$ is the wavenumber of a wave at

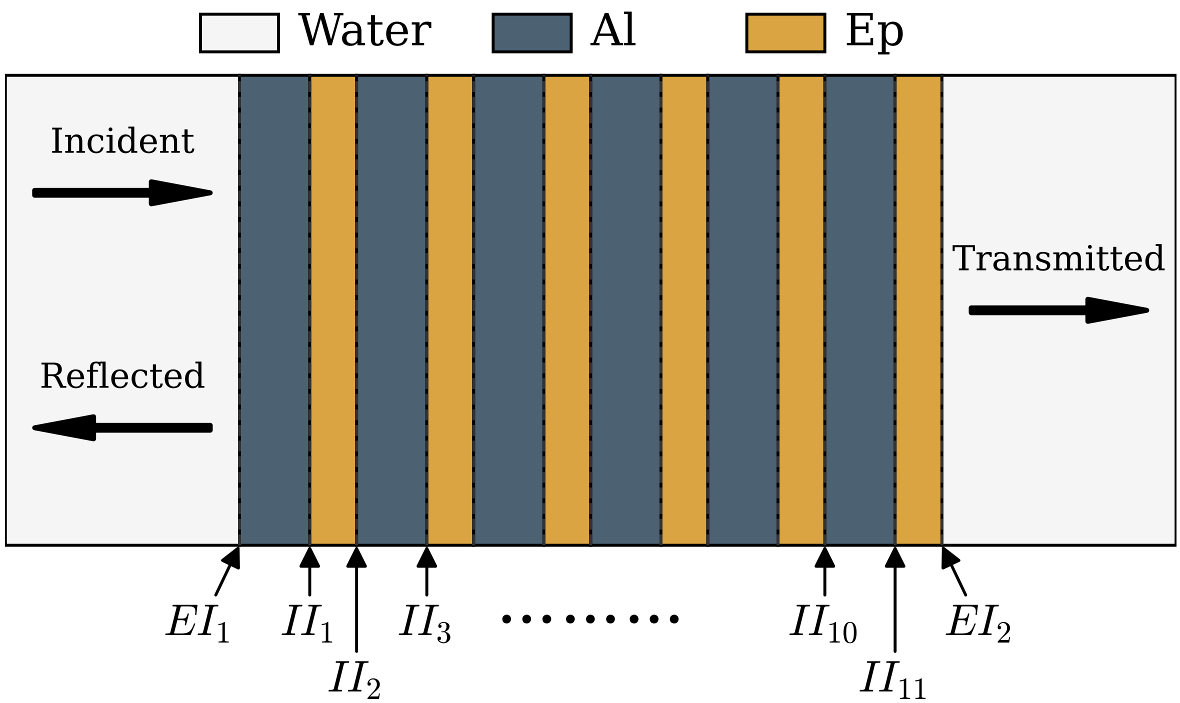

FIG. 3: Six-unit-cell layered structure embedded in water. Γ_1 and Γ_2 denote the external interfaces between water and the layered region, and $I_1, \ldots, I_{11}$ denote the internal Al–Ep interfaces. A wave incident from the left undergoes multiple partial reflections and transmissions at each interface.

frequency f_r in material i. This choice fixes the propagation phase accumulated across each layer at the reference frequency and therefore plays a central role in the interference behavior of the periodic structure, as discussed in the following.

A wave incident from water onto interface Γ_1 is partially reflected and transmitted at this boundary due to the mismatch in the acoustic impedance Z, defined as $Z = \rho c$. The transmitted portion enters the periodic lattice and undergoes further reflections and transmissions at each internal interface. The transmitted field beyond Γ_2 is thus the superposition of many contributions that have followed different paths and accumulated different phases.

The transmission spectrum of the six-unit-cell periodic lattice, designed using the quarter-wavelength condition at the chosen reference frequency $f_r = 1$ MHz, is shown in Fig. 4. The spectrum exhibits a pronounced minimum near this reference frequency, which corresponds to the first stop band of the lattice. To explain the origin of this minimum, we examine both the phase accumulated during propagation within each layer and the phase change upon reflection at each interface.

The reflection coefficient at an interface between media with impedances Z_1 and Z_2 is given by

$$r = \frac{Z_2 - Z_1}{Z_2 + Z_1}. \tag{20}$$

A reflection from a lower-impedance medium to a higher-impedance medium ($Z_2 > Z_1$) gives $r > 0$, corresponding to no phase change, while a reflection from a higher-impedance medium to a lower-impedance medium ($Z_2 < Z_1$) gives $r < 0$, corresponding to a phase reversal of π.

The density ρ and longitudinal wave speed c used in the simulations are listed in Table I.[7,8] These parameters determine the acoustic impedance $Z = \rho c$ of each material. For the present structure, the resulting impedance ordering is

$$Z_{\text{water}} < Z_{\text{Ep}} < Z_{\text{Al}}. \tag{21}$$

As a result, reflections at successive internal interfaces within the periodic Al–Ep lattice alternate between no phase change and a phase reversal.

TABLE I: Material parameters used in the simulations.

Material	Density ρ (kg m^{-3})	Wave speed c (m s^{-1})
Aluminum (Al)	2700	6400
Epoxy (Ep)	1180	2535
Water (W)	1000	1490
Lead (Pb)	11400	1960

We now examine the total accumulated phase change of reflected contributions at the reference frequency f_r as they return to Γ_1. The first reflected contribution arises at Γ_1 (water–Al interface), where reflection occurs without any phase change. The phase change of this reflected wave at Γ_1 is therefore zero.

The next contribution arises from reflection at the first internal interface I_1 (Al–Ep), where a phase shift of π occurs due to reflection from a higher- to a lower-impedance medium.

In addition, the wave propagates through the Al layer to reach I_1 and back to Γ_1, accumulating a total propagation phase

$$2k_{\mathrm{Al}}d_{\mathrm{Al}} = \pi, \tag{22}$$

in accordance with Eq. (19). The total accumulated phase change of this contribution upon returning to Γ_1 is therefore

$$\pi \text{ (propagation)} + \pi \text{ (reflection)} = 2\pi, \tag{23}$$

which is equivalent to zero net phase change.

The next contribution arises from reflection at I_2 (Ep–Al), where no phase change occurs upon reflection. The wave propagates through two layers (Al and Ep) and back, accumulating a total propagation phase

$$2(k_{\mathrm{Al}}d_{\mathrm{Al}} + k_{\mathrm{Ep}}d_{\mathrm{Ep}}) = 2\pi. \tag{24}$$

Thus, this contribution also returns to Γ_1 with zero net phase change.

This phase alignment extends to reflections from deeper interfaces at the reference frequency f_r. The phase changes due to propagation and reflection combine such that each reflected contribution returns to Γ_1 with a total accumulated phase change equal to an integer multiple of 2π.

The transmission spectrum in Fig. 4 illustrates this behavior: the minimum near f_r corresponds to the condition where reflected contributions add coherently and reduce forward transmission, while frequencies away from this condition allow partial transmission. The sharp peaks observed in the pass band arise from interference due to multiple reflections between Γ_1 and Γ_2, analogous to Fabry–Pérot resonances.[9]

The dependence of the transmission spectrum on the number of unit cells is shown in Fig. 5. We plot the transmission spectrum in dB for the same quarter-wavelength lattice designed at $f_r = 1\,\mathrm{MHz}$ for different numbers of unit cells N. As N increases, the transmission within the stop band decreases rapidly and the dip becomes progressively deeper. At f_r, reflected contributions from successive interfaces return in phase, and increasing the number of unit cells adds more such contributions, leading to progressively stronger suppression of transmission through the lattice. At sufficiently large N, the transmitted signal reaches a lower bound set by residual boundary reflections and numerical precision, so that the transmission spectra become difficult to distinguish at very low transmission levels.[§]

[§] The transmission versus N behavior shown here is quantitatively sensitive to the numerical and physical

IV. THE BLOCH LIMIT OF FINITE PERIODIC STRUCTURES

The finite-lattice simulation makes the role of multiple scattering and phase coherence explicit, but it does not provide an explicit connection to the standard analytical description of band formation in infinite periodic media. In the following, we establish this connection by relating the finite-lattice behavior to the Bloch description of an infinite periodic medium.[1,2] Our purpose is to show that the two hallmark Bloch features—exponential attenuation in a stop band and phase accumulation in a pass band—can be directly identified and quantitatively extracted from the finite lattice simulations. This analysis is based on two analytical relations that govern wave propagation in periodic media.

The first relation is the Bloch condition for a periodic medium. For an infinite periodic structure, Bloch's theorem states that the spatial wave field associated with a single frequency component can be written as

$$u(x+a) = u(x)e^{ik_B a}, \tag{25}$$

where $a = d_1 + d_2$ is the unit-cell length and $u(x)$ denotes the spatial wave field. The quantity k_B is the Bloch wavevector, which acts as an effective wavevector of the periodic medium and gives the phase change of the wave across one unit cell of the structure.

The second key relation is the dispersion relation for a bilayer periodic medium under normal incidence of longitudinal elastic waves, commonly known as the Rytov formula.[10–12] The relation is obtained using a transfer-matrix formulation for wave propagation through the layered unit cell, together with the Bloch condition for periodic media. By enforcing continuity of displacement and stress at each interface and relating the wave fields across one unit cell, the resulting dispersion relation is

$$\cos(k_B a) = \cos(k_1 d_1)\cos(k_2 d_2) - \frac{1}{2}\left(\frac{Z_2}{Z_1} + \frac{Z_1}{Z_2}\right)\sin(k_1 d_1)\sin(k_2 d_2), \tag{26}$$

where $k_i = \omega/c_i$ is the local wavenumber in layer i, $\omega = 2\pi f$ is the angular frequency corresponding to the frequency component under consideration, d_i is the layer thickness, and $Z_i = \rho_i c_i$ is the corresponding acoustic impedance.

parameters used in the simulation. Although the overall initial trend of increasing attenuation with increasing number of unit cells should remain unchanged, the details of the spectra may vary depending on the choice of N_{ppw}, α, source bandwidth, source and detector region lengths, and boundary conditions. At very low transmission levels, numerical limits also become important, and the results may no longer clearly distinguish between different cases.

With these two relations, Eqs. (25) and (26), we now examine how the characteristic features of wave propagation in periodic media appear in the finite lattice simulations.

A. Exponential decay in stop band

In Sec. III, stop bands in a finite periodic lattice were identified through a deep minimum in the transmission spectrum. However, a minimum in transmission does not imply that the wave vanishes inside the structure. For frequencies within the stop band, the wave still penetrates the lattice, but its amplitude decreases with depth. Figure 5 provides further insight into this behavior. As the number of unit cells increases, the transmission within the stop band decreases progressively, but remains finite. This reduction reflects spatial attenuation of the wave rather than the absence of the field.

This behavior is captured analytically by the Bloch condition in Eq. (25). Within the band gap frequency range of an infinite periodic lattice, the Bloch wavevector becomes complex and may be written as

$$k_B = k_r + i\kappa, \tag{27}$$

where k_r is the real part of the Bloch wavevector and $\kappa > 0$ denotes the magnitude of its imaginary part. The corresponding Bloch solution no longer represents a propagating wave with constant amplitude. Instead, the wave field acquires an exponential spatial dependence of the form $e^{\pm\kappa x}$, where κ determines the spatial growth or decay rate of the non-propagating mode. In particular, the exponentially decaying branch is commonly referred to as an evanescent Bloch mode. In an ideal infinite lattice, the exponentially growing branch becomes unbounded as $x \to \pm\infty$, and therefore no bounded propagating Bloch mode exists within the band gap.

For the finite lattice, the periodic region extends from the entrance interface Γ_1 to the exit interface Γ_2, as shown in Fig. 3. When the structure is excited from the Γ_1 side, the physically relevant solution corresponds to the forward-decaying branch, and the wave amplitude inside the stop band is approximated by

$$u(x) \sim e^{-\kappa x}, \tag{28}$$

where x is measured from the entrance interface Γ_1. Thus, the absence of propagating Bloch modes in the infinite lattice manifests as exponential spatial attenuation in the finite structure.

To obtain the attenuation constant κ analytically, we consider the infinite lattice dispersion relation given by Eq. (26). The right-hand side of this dispersion relation depends on frequency through the local wavenumbers $k_i = \omega/c_i$. We denote it compactly by $D(\omega)$ and rewrite the relation as

$$\cos(k_B a) = D(\omega). \tag{29}$$

We substitute $k_B = i\kappa$ in the band gap and use $\cos(ix) = \cosh(x)$ to obtain

$$\cosh(\kappa a) = D(\omega), \tag{30}$$

so that

$$\kappa = \frac{1}{a}\cosh^{-1}\big(|D(\omega)|\big). \tag{31}$$

The quantity κ sets the rate at which the wave amplitude decays from one unit cell to the next inside the band gap. Equation (31) provides the analytical attenuation constant associated with the periodic medium.

Our goal is to extract κ numerically from the time-domain simulation in a finite lattice. As a test, we excite a finite Al–Ep lattice using a harmonic source at $f_r = 1\,\mathrm{MHz}$. The layer thicknesses are chosen from the quarter-wavelength condition $d_i = c_i/(4f_r)$ so that this reference frequency lies inside the first stop band. The source is introduced using a smoothly windowed harmonic excitation of the form

$$s(t) = g(t)\sin(2\pi f_r t), \tag{32}$$

where $g(t)$ is a Tukey-type raised-cosine envelope.¶ The envelope smoothly ramps the source amplitude from 0 to 1 near the beginning of the simulation and back to 0 near the end, with taper regions chosen as 20% of the total simulation duration. This smooth windowing suppresses spurious transients and reduces spectral artifacts associated with abruptly switching the source on or off. After a brief transient, the system reaches a steady oscillatory state.

Because the excitation frequency lies inside the stop band, the generated harmonic wave is expected to attenuate as it propagates through the periodic region. This spatial decay is extracted from the steady-state field. If $v(x,t)$ denotes the particle velocity, we evaluate

¶ In the simulation, the envelope function is implemented using the `scipy.signal.windows.tukey` function from the SciPy library.

the root-mean-square (RMS) field over a time window taken during the steady oscillatory portion of the response,

$$v_{\mathrm{RMS}}(x) = \sqrt{\frac{1}{\mathcal{N}} \sum_{j=j_1}^{j_2} v(x, t_j)^2}, \tag{33}$$

where $\mathcal{N} = j_2 - j_1 + 1$ is the number of temporal samples used in the averaging window.

The root-mean-square averaging removes the rapid temporal oscillations of the harmonic field and assigns a single representative amplitude at each spatial location. Thus, $v_{\mathrm{RMS}}(x)$ characterizes the local strength of the oscillatory wave field rather than its instantaneous oscillatory state.

For a harmonic signal, the root-mean-square value is directly proportional to the local amplitude, so it retains the same spatial decay behavior. Therefore, the exponential attenuation in the stop band can be obtained directly from the spatial variation of $v_{\mathrm{RMS}}(x)$.

Because attenuation occurs only inside the periodic lattice, we restrict $v_{\mathrm{RMS}}(x)$ to the periodic region and identify its decaying envelope from the local maxima of its profile. The extracted envelope is fitted using the exponential form

$$v_{\mathrm{env}}(x) = \mathcal{A}\, e^{-\kappa x}, \tag{34}$$

where $v_{\mathrm{env}}(x)$ denotes the envelope of the root-mean-square field, $\mathcal{A}$ is a fitting constant, and κ is the attenuation constant. This κ corresponds to the same quantity obtained analytically from Eq. (31).

Figure 6 shows the resulting spatial profile of the root-mean-square field for an Al–Ep periodic lattice of twelve unit cells. The envelope of the field exhibits clear exponential decay across the periodic region, illustrating the attenuation of the wave inside the stop band.

By applying the fitting procedure to this envelope, we obtain

$$\kappa \approx 786.29\,\mathrm{m}^{-1}, \tag{35}$$

while Eq. (31) gives

$$\kappa \approx 785.16\,\mathrm{m}^{-1}. \tag{36}$$

The relative difference is approximately 0.14%. This close agreement shows that a stop band is not only associated with reduced transmission, but can be characterized quantitatively by a spatial attenuation constant that determines how the wave decays inside the lattice. The extracted decay constant from the finite-lattice simulation agrees with the attenuation constant obtained analytically for an infinite periodic medium, thereby directly connecting the finite-structure dynamics to the Bloch description. In this sense, the observed decay corresponds to a non-propagating wave mode within the periodic lattice, characterized by an exponential attenuation of the wave amplitude with distance. This behavior is indicative of an evanescent wave in a periodic medium.

B. Bloch Dispersion Relation

We now consider the complementary Bloch feature associated with pass bands: the phase accumulation of the wave across successive unit cells of the periodic lattice. For frequencies within the pass bands, waves propagate through the structure while maintaining a definite phase relation from one unit cell to the next. This behavior is reflected in Eq. (29), where $|D(\omega)| \leq 1$ corresponds to pass bands with real values of k_B and hence a well-defined phase advance across the lattice; $|D(\omega)| > 1$ implies that no real Bloch wavevector satisfies the relation and therefore corresponds to band gaps. The relation between the frequency and the Bloch wavevector obtained from Eq. (29) defines the dispersion relation of the periodic medium. We now examine how this dispersion can be extracted directly from time-domain simulations of a finite lattice.

We make use of the Bloch condition in Eq. (25). Inside the periodic region of the lattice, neighboring unit cells have the same material arrangement, so the wave field evolves from one cell to the next through a repeated phase relation characterized by the Bloch wavevector. The Bloch condition states that field values at locations separated by one unit cell differ only by a phase factor determined by the Bloch wavevector. We apply the Bloch condition to the spatial locations $x - a$, x, and $x + a$ within the periodic region and find

$$u(x + a) = u(x)e^{ik_B a}, \tag{37}$$

and

$$u(x - a) = u(x)e^{-ik_B a}. \tag{38}$$

We add Eqs. (37) and (38) to obtain

$$u(x - a) + u(x + a) = 2\cos(k_B a)\, u(x), \tag{39}$$

from which we find

$$\cos(k_B a) = \frac{u(x-a) + u(x+a)}{2u(x)}. \tag{40}$$

This relation therefore provides a direct way to determine the Bloch phase advance across one unit cell from field values measured within the finite lattice.

To obtain frequency-dependent information, we work in the frequency domain. Let $v_1(\omega)$, $v_2(\omega)$, and $v_3(\omega)$ denote the temporal Fourier transforms of the velocity signals measured at $x-a$, x, and $x+a$ within the periodic region. The three-point relation then becomes

$$\cos(k_B a) = \frac{v_1(\omega) + v_3(\omega)}{2\, v_2(\omega)}. \tag{41}$$

To improve robustness, the frequency-domain relation given by Eq. (41) is evaluated using multiple triplets located within the interior of the lattice, each separated by one unit cell and chosen sufficiently far from the outer boundaries to reduce reflection effects. The resulting values of $\cos(k_B a)$ are then averaged over all such triplets and compared directly with the analytical prediction from Eq. (26).

Figure 7 compares the dispersion relation extracted from the finite-lattice simulation of a 12-unit-cell periodic structure with the analytical prediction from the Rytov formula. The excellent agreement across the pass bands, together with the emergence of gaps near the Brillouin-zone boundary ($k_B a = \pi$), shows that the phase evolution predicted by the Bloch theory can be determined from finite-lattice time-domain simulations. The results show that the dispersion relation is already encoded in the local phase evolution of waves propagating through a finite periodic lattice. By tracking how the phase accumulates across successive unit cells, the finite-lattice simulation reproduces the same frequency–wavevector relation that is obtained from analytical treatments of infinite periodic media.

Taken together, these results establish a direct connection between the finite-lattice wave dynamics observed in the simulations and the Bloch description of an infinite periodic medium. In the finite periodic lattice, repeated scattering across many interfaces produces two distinct forms of wave behavior. For frequencies inside the stop band, the simulated wave field exhibits exponential spatial attenuation within the lattice. This decay is quantitatively governed by the same attenuation constant κ obtained from the Bloch description of an infinite periodic medium. For frequencies inside the pass bands, the simulated fields maintain a definite phase relation across successive unit cells, allowing the Bloch dispersion relation associated with an infinite periodic medium to be extracted directly from the finite-lattice dynamics. The time-domain simulation therefore recovers the same physical behavior predicted by the Bloch description of an infinite periodic medium, without invoking infinite periodicity. In this way, the characteristic features of band formation emerge naturally from wave propagation through a finite layered lattice.

V. SUMMARY

We have presented a compact computational framework for reconstructing band formation in periodic media directly from time-domain wave dynamics in finite layered systems. Starting from repeated reflections at material interfaces, the simulations show how interference and phase accumulation give rise to pass bands and stop bands, characterized by strong transmission and attenuation, respectively. As the number of unit cells increases, the attenuation within the stop bands becomes stronger, consistent with exponential spatial decay, and the phase advance across successive unit cells provides direct access to the dispersion relation.

This approach establishes a direct connection between finite-structure dynamics and Bloch theory without assuming infinite periodicity at the outset. In this way, band structure emerges naturally from real-space wave propagation, offering a physically transparent route to understanding wave behavior in periodic media.

Our approach can be incorporated into undergraduate computational courses in which students reconstruct dispersion relations directly from time-domain data. The emergence of complex wavevectors in stop bands offers an intuitive way to visualize evanescent modes, a concept that is often abstract in traditional treatments. More broadly, this approach shows how band structure can be inferred from local measurements, providing a natural entry point to inverse problems in wave physics and to modern wave-based materials such as photonic ** and phononic crystals.[13]

** Photonic crystals are periodic optical materials in which spatial variations in refractive index produce photonic band gaps that control the propagation of electromagnetic waves.

VI. SUGGESTED PROBLEMS

The following problems are designed to guide students in exploring the emergence of band formation in periodic media. Students are encouraged to make qualitative predictions before performing the simulations, and to interpret their results in terms of interference, phase coherence, and wave propagation.

1. **Breakdown of periodicity:** Band gaps in periodic media arise from coherent multiple scattering across identical unit cells. This problem examines how deviations from perfect periodicity modify this coherence and alter the transmission characteristics of the lattice.

   (a) *Local perturbation (single defect).* Construct a short periodic lattice consisting of six unit cells using the quarter-wavelength design described in the text. Introduce a local defect by modifying a single layer while keeping the remainder of the structure unchanged. First double the thickness of an epoxy layer near the center of the six-unit-cell lattice so that the defect remains well separated from the outer boundaries. (i) How would you expect a single defect to affect transmission within the stop band? Compute the transmission spectrum and compare it with that of the unperturbed lattice. Identify any transmission peaks that appear within the stop band. Explain the origin of these features in terms of phase accumulation and the local disruption of destructive interference near the defect. (ii) Increase the size of the lattice while keeping the defect near the center of the structure, and examine how the defect-induced transmission peak and localization behavior change. Then increase the total simulation time by using at least twice the number of time steps and observe how the transmission spectrum changes. Explain the role of localization, attenuation, and finite simulation time in the behavior of the larger lattices. (iii) Relate the localized transmission mode to the concept of impurity-induced states inside the band gap of semiconductors.

   An implementation corresponding to this problem is provided in the script `P1_DefectState_LocalizedTransmission.py`, included in the Supplemental Material.

   (b) *Distributed perturbations (weak disorder).* Introduce weak disorder by applying small random variations to all layer thicknesses:

$$d_i \to d_i(1 + \eta_i), \qquad \eta_i \in [-\delta, \delta]. \tag{42}$$

(i) How is weak disorder expected to affect phase coherence across successive unit cells? Compute the transmission spectrum for increasing disorder strengths δ (e.g., beginning with 5%). Examine how the width and depth of the stop band evolve. Discuss your results in terms of the gradual loss of phase coherence. (ii) For a fixed disorder strength, investigate how increasing the number of unit cells affects the transmission spectrum. What does your results suggest about the role of multiple scattering? (iii) Examine whether signatures of disorder can be identified directly from the transmission spectrum.

An implementation corresponding to this problem is provided in the script `P2_DisorderedLattice_Transmission.py`, included in the Supplemental Material.

2. **Role of impedance contrast and band gap tailoring:** The strength of wave reflection at an interface depends on the acoustic impedance mismatch between adjacent layers. This problem investigates how impedance contrast influences stop-band formation.

   (a) *Comparison of material pairs from Table I.* Construct periodic lattices using different pairs of materials (for example, epoxy–water, aluminum–epoxy, and lead–epoxy), while keeping the number of unit cells and the quarter-wavelength design frequency the same. (i) How does increasing impedance contrast affect the width and depth of the stop band? Compute and compare the transmission spectra for the different structures. Examine how the stop band characteristics vary with material combination. Explain your observations in terms of reflection strength and multiple scattering within the lattice. (ii) Relate your observations to the reflection coefficient at a single interface. Discuss how increasing impedance contrast modifies the cumulative effect of multiple reflections. Reproduce the results of Sec. IV for each structure and examine how the impedance contrast influences the attenuation within the stop bands and the dispersion behavior in each case.

(b) *Band gap design.* Use the materials provided in Table I to design periodic layered structures to achieve the following objectives: (i) A structure with a wide and strongly attenuating stop band near a chosen frequency. (ii) A structure with a narrow and sharply defined stop band exhibiting high spectral selectivity. For each design, predict how your choice of materials and layer thickness will influence the band structure and then compute and plot the transmission spectrum. Explain how impedance contrast, layer thickness, and phase accumulation contribute to the observed behavior.

(c) *Identifying periodicity from spectra.* Consider a transmission spectrum exhibiting a pronounced stop band. (i) What features of the spectrum suggest the presence of periodic layering? (ii) Using your results from Problem 1, determine whether signatures of broken periodicity or structural disorder can be identified directly from the transmission spectrum. (iii) Which spectral features are most sensitive to phase coherence across successive unit cells?

AUTHOR DECLARATIONS

The authors declare that they have no conflicts of interest.

Appendix A: Mur's Absorbing Boundary Condition

To model an effectively unbounded medium within a finite computational domain, absorbing boundary conditions are applied at the domain edges to suppress artificial reflections. In this work, we use Mur's first-order absorbing boundary condition.

Consider the one-dimensional wave equation for a field $u(x,t)$ propagating in a homogeneous medium with wave speed c,

$$\frac{\partial^2 u}{\partial t^2} = c^2 \frac{\partial^2 u}{\partial x^2}. \tag{A1}$$

Equation (A1) can be factorized as

$$\left(\frac{\partial}{\partial t} - c\frac{\partial}{\partial x}\right)\left(\frac{\partial}{\partial t} + c\frac{\partial}{\partial x}\right) u(x,t) = 0, \tag{A2}$$

which represents a superposition of left- and right-traveling waves. The corresponding one-way wave equations are

$$\frac{\partial u}{\partial t} - c\frac{\partial u}{\partial x} = 0 \quad \text{(left-moving wave)}, \tag{A3}$$

$$\frac{\partial u}{\partial t} + c\frac{\partial u}{\partial x} = 0 \quad \text{(right-moving wave)}. \tag{A4}$$

At the boundaries of a finite computational domain, only outgoing waves should be present. Therefore, at the left boundary ($x = x_0$), we impose the left-moving wave equation, and at the right boundary ($x = x_M$), the right-moving wave equation. To obtain discrete update relations, the derivatives are approximated using centered differences in both space and time at half steps. This approximation yields the boundary update relations[14]

$$u_0^{n+1} = u_1^n + \frac{r-1}{r+1}\left(u_1^{n+1} - u_0^n\right), \tag{A5}$$

$$u_M^{n+1} = u_{M-1}^n + \frac{r-1}{r+1}\left(u_{M-1}^{n+1} - u_M^n\right). \tag{A6}$$

Here, $r = c\Delta t/\Delta x$ is the local Courant number, where c denotes the wave speed in the homogeneous surrounding medium adjacent to the computational boundaries. Because the particle velocity $v = \partial u/\partial t$ also satisfies the wave equation in Eq. (A1), these boundary updates are applied directly to the velocity field at the domain edges.

[1] C. Kittel, *Introduction to Solid State Physics*, 8th ed. (Wiley, 2004).

[2] N. W. Ashcroft and N. D. Mermin, *Solid State Physics* (Holt, Rinehart and Winston, 1976).

[3] A. Taflove and S. C. Hagness, *Computational Electrodynamics: The Finite-Difference Time-Domain Method* (Artech House, 2005).

[4] J. D. Achenbach, *Wave Propagation in Elastic Solids* (Elsevier Science, 2012).

[5] L. D. Landau, E. M. Lifshitz, A. M. Kosevich, and L. P. Pitaevskii, *Theory of Elasticity: Volume 7* (Butterworth-Heinemann, 1986).

[6] K. S. Yee, "Numerical solution of initial boundary value problems involving Maxwell's equations in isotropic media," IEEE Trans. Antennas Propag. **14** (3), 302–307 (1966).

[7] A. H. Aly, A. Nagaty, and A. Mehaney, "Thermal properties of one-dimensional piezoelectric phononic crystal," Eur. Phys. J. B **91** (10), 251 (2018).

[8] A. Mehaney and A. M. Ahmed, "Locally resonant phononic crystals at low frequencies based on porous SiC multilayer," Sci. Rep. **9** (1), 14767 (2019).

[9] M. Born, E. Wolf, and A. B. Bhatia, *Principles of Optics: Electromagnetic Theory of Propagation, Interference and Diffraction of Light* (Cambridge University Press, 1999).

[10] S. M. Rytov, “Electromagnetic properties of a finely stratified medium,” Sov. Phys. JETP **2** (3), 466–475 (1956).

[11] L. M. Brekhovskikh, *Waves in Layered Media*, 2nd ed. (Academic Press, New York, 1980).

[12] P. Yeh, *Optical Waves in Layered Media* (Wiley, 2005).

[13] A. R. McGurn, *Introduction to Photonic and Phononic Crystals and Metamaterials* (Morgan & Claypool, 2022).

[14] G. Mur, “Absorbing boundary conditions for the finite-difference approximation of the time-domain electromagnetic-field equations,” IEEE Trans. Electromagn. Compat. **23** (4), 377–382 (1981).

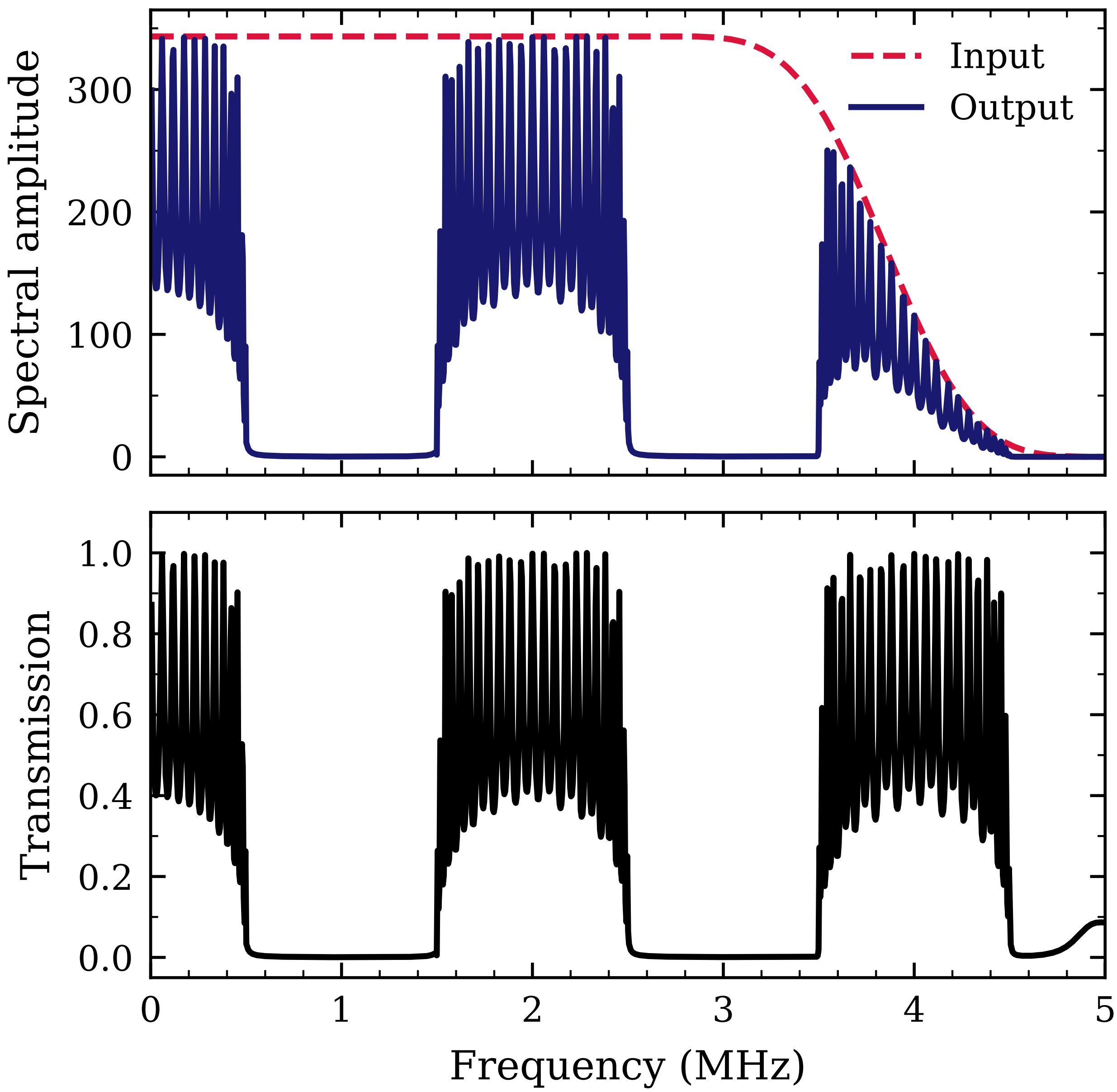

FIG. 4: (a) Frequency spectra obtained from simulations without lattice (dashed) and with lattice (solid) for a broadband Ricker wavelet excitation with central frequency $f_c = 0.3 f_{\max}$, where $f_{\max} = 5.5$ MHz, and time delay $t_c = 3/f_c$. The source and sampling regions in the surrounding medium are each chosen to be five times the unit-cell length. The source is placed at the center of the surrounding region before interface Γ_1, and the transmitted signal is recorded one unit cell length beyond interface Γ_2. (b) Transmission spectrum obtained by normalizing the spectrum from the lattice case with respect to the homogeneous (without lattice) case. Broad minima near $f_r = 1$ MHz arise from interference within the layered structure, while sharp resonances are due to multiple reflections between the external interfaces

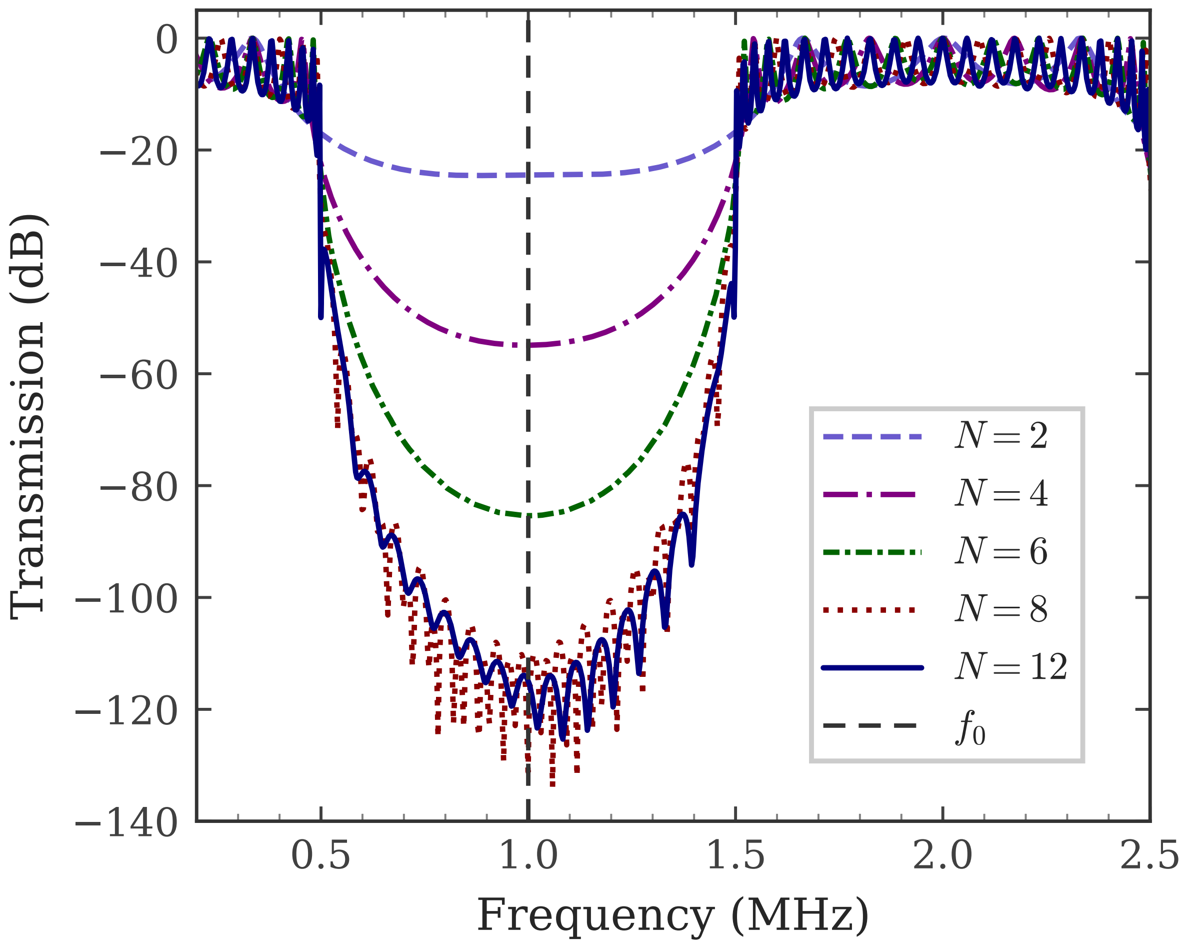

FIG. 5: Transmission spectra in dB for increasing number of unit cells N in the quarter-wavelength lattice designed at $f_r = 1$ MHz. The surrounding medium on both sides of the lattice is chosen to be ten times the unit-cell length. The stop band at f_r shows progressively stronger attenuation due to multiple scattering. At sufficiently large N, the transmitted signal reaches a lower bound set by residual boundary reflections and numerical precision, making the spectra difficult to distinguish at very low transmission levels.

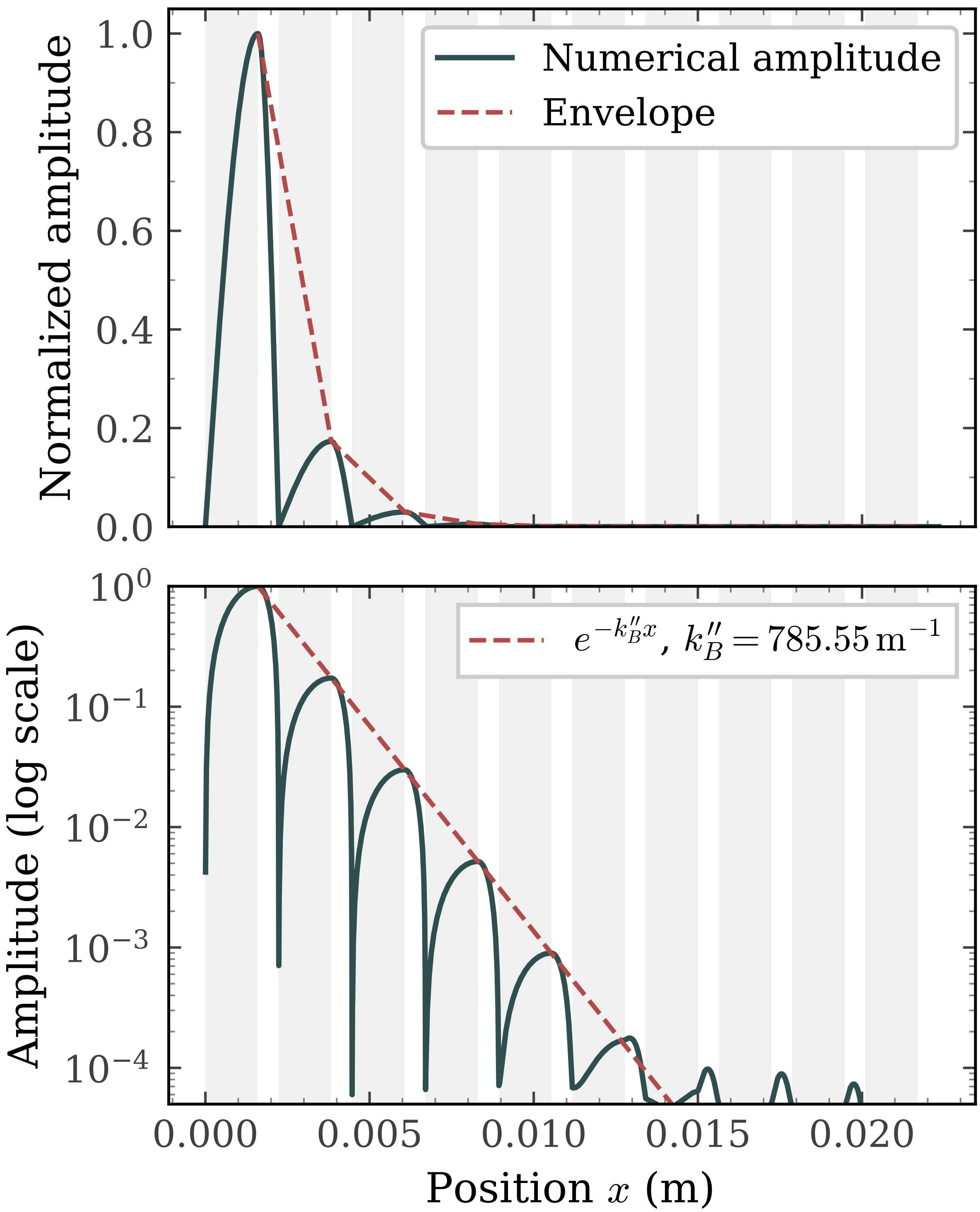

FIG. 6: Spatial variation of the root-mean-square amplitude inside a twelve-unit-cell Al–Ep periodic lattice for harmonic excitation at $f_r = 1\,\mathrm{MHz}$, corresponding to a frequency in the stop band. (a) Normalized root-mean-square amplitude showing the rapid decay within the lattice. (b) The same data on a logarithmic scale clearly illustrates the exponential attenuation behavior. The dotted curve represents the exponential fit applied to the extracted envelope of the amplitude.

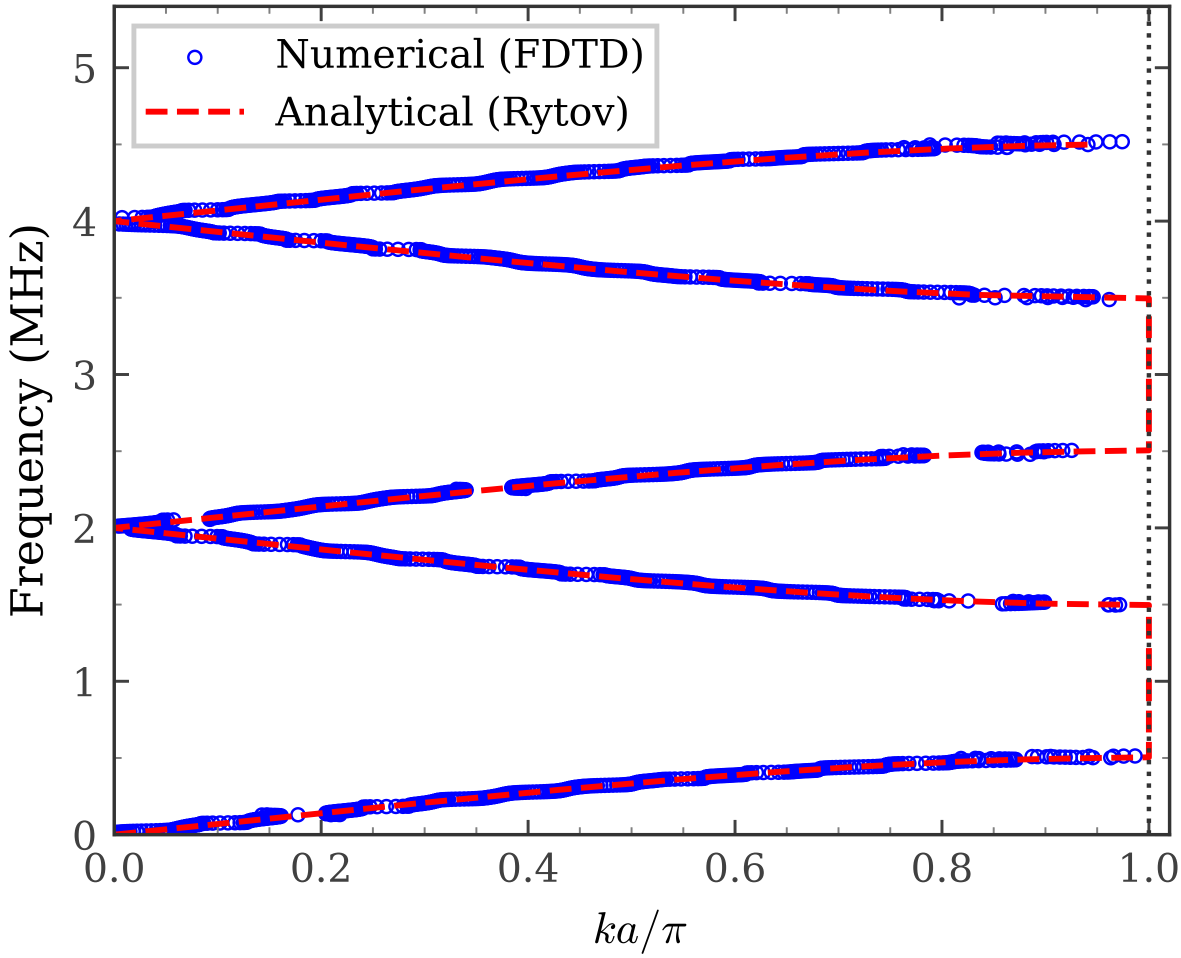

FIG. 7: Comparison of the analytical dispersion relation (Rytov formula, red dashed curves) and the Bloch wavevector extracted from finite-lattice simulations (blue circles) for a 12-unit-cell Al–Ep periodic lattice designed using the quarter-wavelength condition at the reference frequency $f_r = 1\,\mathrm{MHz}$. The numerical results are obtained using a broadband Ricker wavelet excitation with central frequency $f_c = 6.5\,\mathrm{MHz}$. The Bloch wavevector is extracted using the three-point Bloch relation evaluated over four interior sampling triplets, each separated by one unit cell and chosen away from the outer boundaries to minimize boundary-reflection effects. The horizontal axis shows the normalized Bloch wavevector $k_B a/\pi$. The shaded regions indicate frequency ranges where no real Bloch wavevector exists, corresponding to stop bands characterized by exponential attenuation inside the periodic lattice.